MARES Project: Hydrographic data of the San Jorge Gulf from R/V *Coriolis II* cruise in 2014.

Juan Cruz Carbajal[1], Marcela Charo[2], Andrés Luján Rivas[1], and Cédric Chavanne[3]

[1]Centro para el Estudio de Sistemas Marinos, CONICET, Chubut, Argentina
[2]Departamento Oceanografía, Servicio Hidrografía Naval, Buenos Aires, Argentina
[3]Institut des sciences de la mer de Rimouski, Université du Québec à Rimouski, Canada

Correspondence to: Juan Cruz Carbajal (carbajaljuancruz@gmail.com)

Abstract. PROMESse (Multidisciplinary program for the study of the ecosystem and marine geology of San Jorge Gulf and the coast of the Province of Chubut) was an international cooperation research program between the Ministry of Science and Technology (MINCyT), the National Scientific and Technical Research Council (CONICET), the Province of Chubut (Argentina) and the University of Québec at Rimouski (UQAR/ISMER, Canada). Within the framework of this program two projects were carried out, MARES (Marine Ecosystem Health of the San Jorge Gulf: Present status and Resilience capacity) and MARGES (Marine Geology). The main goal of MARES was to drive a comprehensive study of the dynamics of physical, chemical and biological parameters, which are vital for the San Jorge Gulf ecosystem. The observational component of this project consisted on a multidisciplinary oceanographic cruise on board of the research vessel *Coriolis II* in Feb. 2014 integrated by three legs designed to identify and characterize areas of high primary productivity that will serve as indicators of the ecosystem's health. This paper reports the hydrographic data collected during the second leg of the *Coriolis II* cruise. This leg's aim was to study the frontal dynamics associated to a region of high tidal dissipation rate south of the Gulf and to study the vertical displacements of the pycnocline at a fixed site in the center of the Gulf mouth. To this end, high-resolution data (Scanfish II) and quasi-continuous CTD vertical profiles were collected in the southern tidal front, and 'yo-yo' CTD casts were occupied at a fixed location. Moreover, complementary data from underway surface CTD and shipboard ADCP were collected during the cruise. The data sets are available in the National Oceanographic Data Center (NODC) from NOAA. DOI: https://doi.org/10.7289/V5MP51J2

1 Introduction

The Patagonian Shelf is ranked as the fifth most shallow sea region in the global distribution of tidal energy dissipation, accounting nearly 112 GW for the M2 tidal component and is known for its large tidal amplitudes and the speed of the tidal wave (Egbert and Ray, 2001; Simpson and Bowers, 1981; Glorioso and Flather, 1995, 1997; Miller, 1966; Cartwright and Ray, 1991; Webb, 1973; Forbes and Garraffo, 1988; Rivas, 1994). It is also the host of extremely rich persistent-and-seasonal frontal systems (Acha et al., 2004; Campagna et al., 2007; Belkin et al., 2009; Romero et al., 2006; Miloslavich et al., 2011; Alemany et al., 2009).

The San Jorge Gulf (SJG) is the largest semi-open basin located in Patagonian Shelf (approximately 40000 km^2), the most productive hydrocarbon (oil and gas) basin of Argentina and represents an important hydrocarbon reserves (Sylwan, 2001). It is located between 45° S and 47° S with depths slightly over 100 m in the central region (Fig. 1). Its broad mouth extends 230 km from Bahía San Gregorio to Cabo Tres Puntas along the meridian 65° 45' W, connecting the Gulf with the Argentine Continental Shelf through a sill that increases in the S-N direction, reaching a maximum depth of ~ 60 m near 46° 48' S (Fig. 1). This geomorphological feature in interaction with the strong tidal currents increase near-bottom mixing that reaches the sea surface and produces changes of well-stratified conditions to well-mixed conditions within a few kilometers during the warm seasons.

The SJG circulation is driven by intense westerly winds and high amplitude tides (Palma et al., 2004; Tonini et al., 2006; Moreira et al., 2011). Estimates of tidal energy dissipation by bottom friction derived from numerical models results (Glorioso and Flather, 1995, 1997; Palma et al., 2004; Moreira et al., 2011) suggest that most of the dissipation occurs at the mouth of the SJG, mainly in the southeast region. The dissipation rate is high enough to break up the seasonal thermocline and give rise to the formation of an intense tidal front.

Due to its configuration and variability (Carbajal et al., 2018), the tidal front enhances the biological productivity nearby (Glembocki et al., 2015), plays a key role in the development of ecological processes and is closely related to fishery resources (Acha et al., 2015; Alemany et al., 2014). Studying the frontal variability, both spatial and temporal, is essential to understand the mechanism responsible for that enhancement and to define main frontal properties related to biological effects. Thus, the use of a high-resolution sampler system was key to evidence the high-frequency frontal variability. Knowledge of mesoscale variability is not only crucial to interpreting the biological influence of the fronts (Landeira et al., 2014), but it will also contribute to the establishment of new conservation strategies and the management of marine resources.

In this article we describe the cruise's design and the procedures used for the acquisition (Sect. 2), calibration (Sect. 3 and Sect. 4) and processing (Sect. 5) of the data set obtained during MARES leg 2. Furthermore, data gridding procedures of one high-resolution section collected during the frontal survey are presented in Appendix A.

2 Field measurements and equipment

Two types of surveys were carried out between Feb. 4-10 2014 on board of the Canadian research vessel (R/V) *Coriolis II* during MARES leg 2 cruise: one located in the STF region (Sect. 2.1) and another in a fixed position near the center of the Gulf mouth (Sect. 2.2). Complementary observations were also accomplished (Sect. 2.3). While towed undulating vehicle systems have been used by investigators (Twardowski et al., 2005; Brown et al., 1996), the PROMESse program was the ideal framework for the application of new technologies in Patagonian Shelf such as this vehicle, achieving unprecedented high temporal and spatial resolution data in the region, particularly in the STF. After the *Coriolis II* cruise, two surveys were carried out in the SJG (during Nov.2016 and Oct-Nov.2017) in the framework of a national project in which the towed undulating vehicle was not available. Thereby, the focus of this article is on the originality of the data set to study the high-frequency frontal dynamics.

Table 1 summarizes the characteristics of the sensors used in each instrument. Date and time from data sets are reported in Coordinated Universal Time (UTC).

2.1 Southern Tidal Front observations

Eighteen cross-front transects (six in late spring tide (Feb. 5), six in intermediate tide (Feb. 8-9) and six in early neap tide (Feb. 9-10) were occupied in the STF using a towed undulating vehicle EIVA Marine Survey Solutions model Scanfish II (http://aquaticcommons.org/3106/1/ACT_WR07-01_Tower_Vehicles.pdf), fitted with a modular CTD Sea-Bird Electronic (SBE) model 49FastCAT (16 Hz) and a combined fluorometer and turbidity sensor WetLabs model ECO FLNTU (8 Hz). The modular CTD has no memory nor internal batteries, and does not support auxiliary sensor inputs either. Therefore, the ECO FLNTU could not be directly associated with the CTD data during the surveys and thus the fluorescence and turbidity signal was acquired without the corresponding date, time and position. Nevertheless, it was possible to link both signals to get the missing data in a post-processing using complete data (date, time and position) of Scanfish CTD and the sampling intervals of the two sensors employed simultaneously to link the missing data to the corresponding record of the FLNTU data. The sections length ranged between 17.4 km to 63.1 km, which is equivalent to 1:09 h and 4:33 h of transit (see Table 2 for details). The sections occupied in late spring and early neap tide covered an area of approximately 29.8 km (NW-SE) by 15.1 km (NE-SW) during a semi-diurnal tidal cycle each (Figs. 1c and 1e, respectively), while the intermediate tide survey consisted of a single transect (T1) occupied six times, back and forth, also during a semi-diurnal tidal cycle (Fig. 1d). Surveys detail above are shown in Fig. 1. It is worth pointing out that the sampling experience shows that carrying out the same cross-front transect several times is recommendable (e.g. Fig. 1d) given that the along-front variability (ruled by baroclinic instabilities) difficult the prediction of the front´s location during the early neap tide and that the cross-frontal physical mechanisms (ruled by the tide) of interest do not change much at this scales. The horizontal separation of Scanfish sawtooth profiles was approximately 81 m–291 m, the latter largely dependent on bottom depth and the condition in the sea surface, descending (ascending) the vehicle at an absolute rate of nearly 0.9 $\mathrm{m\ s^{-1}}$. On board, the towed vehicle was monitored through the roll and pitch sensors. The vehicle attitude was governed through two rear-mounted flaps and depths were provided by the CTD pressure sensor (Brown et al., 1996). The data collected with the Scanfish II provided a quasi-synoptic spatial and temporal resolution to characterize the influence of the high/low tide behavior and determine the front displacements relative to the phase of the tide.

An additional cross-frontal transect was occupied across the STF (on Feb. 5 at night and Feb. 8 at late afternoon) to study the biological and chemical characteristics of the water column. Each realization consisted of five quasi-continuous full depth CTD-rosette casts spaced at distance intervals of ~ 4.9 km, using a CTD SBE model SBE911*plus*, equipped with oxygen, pH, fluorescence, nutrients, photosynthetically active radiation (PAR), beam transmission and altimeter sensors (Table 1). The altimeter sensor was used to determine distance to the bottom. Most vertical profiles reached to within ~ 9 m off the bottom. Oxygen, pH and fluorescence sensors were calibrated based on water samples from Niskin bottles as described in Sect. 3. Data from the remaining sensors are reported based on factory calibrations only. Down profiles are reported in this data set because during downcast the CTD sensors measure the water column with minimal interference from the underwater package.

2.2 Fix Station observations

From Feb. 6 2014 17:04 h UTC to Feb. 8 2014 04:01 h UTC, a time series was carried out in a fixed station (FS) near to the center of the SJG mouth (45° 56' S, 65° 33' W). The time series consisted of thirteen quasi-continuous full depth CTD-rosette casts collected approximately every 2:55 h during 34:57 h using the CTD SBE911*plus*. The objective of this survey was to monitor the pycnocline displacements in the water column and to determine the mechanisms responsible for these vertical movements. It is expected that these mechanisms could be similar to that observed in the STF and will allow to identify vertical stratification variations in the water column which could affect the productivity in the frontal region.

2.3 Complementary observations

An underway CTD SBE model SBE19*plus* (4 Hz) coupled with a Seapoint fluorescence sensor was used to identify the position and orientation of the STF and remained operational throughout the entire cruise (Sect. 6). The real-time sample interval of the underway was set to 0.25 s along the tracks. Direct velocity measurements were collected with a Teledyne RD Instruments (TRDI) 150 kHz Ocean Surveyor hull-mounted Acoustic Doppler Current Profiler (ADCP, Sect. 7). These data sets are reported in the data collection.

3 Water Samples

A Carousel Sea-Bird model SBE32 rosette package with twelve 12 L Niskin bottles was employed during the cruise. At pre-defined depths, water samples were collected for the determination of salinity, dissolved oxygen (DO), nutrients, pH and chlorophyll-a (Chl) concentrations in the water column. In addition, they were used to calibrate the ancillary sensors of the CTD, as showed in Sect. 4.2.

Due to the lack of a salinometer on board, salinity water samples were drawn in small glass flasks and sealed with insulation tape. Fourteen days after the cruise ended, salinity samples were determined at the Instituto Nacional de Investigación y Desarrollo Pesquero (INIDEP) with a Guildline Autosal 8400B salinometer based on the technical specifications of the manual (Guildline Instruments, 2004). All salinity samples showed a positive bias (0.009±0.007 psu, $N = 35$) when compared to CTD salinity values. The water samples most likely experienced evaporation during this period and therefore the salinity measurements were overestimated. Bottle salinity data were considered questionable, and because the CTD conductivity sensor was factory calibrated in 2013, the bottle salinity data were not used to calibrate it. Salinity values were calculated and reported in Practical Salinity Units (UNESCO IWG, 1981).

DO water samples were drawn in DBO glass bottles with frosted neck to avoid evaporation. DO concentrations were determined with a modified Winkler method (Carpenter, 1965) using an automatic Metrohm volumetric titrator.

Nutrients water samples were drawn in 250 ml plastic bottles and frozen immediately at -20° C without previous filtration, until they were analyzed at the Laboratorio de Oceanografía Química y Contaminación de Aguas (LOQyCA) of the Centro Nacional Patagónico (CENPAT). Analysis of four macro-nutrients (nitrate, nitrite, silicate and phosphate) concentrations were

determined using colorimetric techniques on Skalar San Plus autoanalyser (Skalar Analytical® V.B, 2005a, b, c), according to the methods described in Strickland and Parsons (1972).

Chl concentrations were determined fluorometrically by filtering 500 to 1500 ml seawater samples through 25 mm Whatman GF/F (0.7 $\mu\mathrm{m}$ porosity) glass fiber filters. Chl and phaeopigments were extracted on board in 90 % acetone for a period of 12 to 24 h in the dark. Fluorescence measurements were performed on board in the dark with a Turner Designs model 10-AU fluorometer according to the Parsons et al. (1984) method.

pH of water samples were measured on board using a YSI 556 MSI multiparameter probe.

Nutrients, DO, chl and pH data from the water samples collected in MARES leg 2 cruise were compared with historical data available in the Argentine Oceanographic Data Center (CEADO, http://www.hidro.gov.ar/ceado/ceado.asp) for austral summer (Jan-Feb-Mar) in the region of interest. CEADO archives data originated by national and international research institutions. Water samples observations were consistent with historical observations.

4 Sensor calibrations

4.1 Scanfish II CTD calibration

In April 2015, the SBE49FastCAT sensor was sent to SBE factory for the post-cruise calibration. Thus, the pre- and post-cruise calibration was used to generate a *slope* (in conductivity) and an *offset* (in temperature) corrections for these data, following Sea-Bird Electronics Inc (2010). The laboratory calibration showed drift corrections of -0.00010 $\mathrm{psu\ month}^{-1}$ and -0.00017 $^{\circ}\mathrm{C\ year}^{-1}$; corresponding to a conductivity *slope* value of 1.00010 and a temperature *offset* value of 0.00052 $^{\circ}\mathrm{C}$, respectively. Fluorescence and turbidity data from the ECO FLNTU sensor are reported based on factory calibrations only.

4.2 CTD ancillary sensors calibration

The SBE43 oxygen sensor has a very stable electronic system, therefore, any loss of its accuracy with time is primarily attributed to fouling of the membrane, either biological or waterborne contaminants (e.g., oil). The manufacturer provides an algorithm to adjust the drift by using a quality reference sample such as Winkler titrated and the SBE43 measured DO concentrations at the times the water samples were collected (Sea-Bird Electronics Inc, 2012). DO differences greater than one standard deviation were discarded and not used in the DO sensor calibration. The standard deviation of the residuals after calibration was approximately 0.08 $\mathrm{ml\,l}^{-1}$ ($N = 48, DO(\mu\mathrm{mol/kg}) = 44660 \cdot DO(\mathrm{ml/l})/(\sigma_{theta} + 1000)$). Figure 2 presents the residual (CTD DO - Winkler DO) before and after calibration.

The MBARI-ISUS sensor is designed mainly to determine nitrate concentrations in the 200-400 nm range of the ultraviolet-spectrum, as the main nutrients required for growth of phytoplankton (Satlantic LP, 2012). A post-cruise inspection of the vertical distribution of nitrate together with the nutrients water samples were carried out in the frontal zone and in the FS. The analysis suggested that the nutrient sensor did not work properly, showing negative values of nitrates in some profiles. Thus, the data of this sensor are reported based on its factory calibration.

The fluorescence sensor calibration was performed using a linear adjustment with Chl concentration from water samples to obtain the calibration coefficients. In the same way, pH water samples were fitted to pH sensor data. The squared correlation coefficient and the standard deviations post-calibration were $R^2 = 0.891$ ($N = 37$), $0.233\ \mathrm{mg\ m^{-3}}$ and $R^2 = 0.908$ ($N = 54$), 0.049, respectively.

5 Scanfish II and CTD data processing

Scanfish and CTD data were post-processed using SBE Data Processing software routines (v. 7.23.2, Seasoft-Win32, http://www.seabird.com/software/software). The processing sequence for the SBE911*plus* did not follow the *typical* sequences suggested by the manufacturer because the 'scans to average' parameter was set to 24 in the configuration file used on board and so the raw vertical profiles were stored at 1 Hz averages. SBE technical support suggested skipping any filter steps, since the data was already averaged (see SBE manual for details, http://www.seabird.com/sites/default/files/documents/SBEDataProcessing_7.26.4.pdf). The Deck Unit was programmed to advance conductivity 0.073 s relative to pressure. Because oxygen data is also systematically delayed with respect to pressure, several tests were carried out to determine the best aligment, which was set to +3 s. Each CTD profile was then inspected and density inversions were removed and filled in by a linear interpolation of the original temperature and conductivity data. All derived parameters were recalculated at the interpolated pressure and then the final data were averaged at 1 dbar pressure intervals.

The processing sequence for the SBE49FastCAT was based on the manufacturer suggestions. Raw temperature and conductivity data are often misaligned with respect to pressure in areas with strong vertical stratification due to vertical temperature gradient, causing spikes in derived variables, mainly in salinity. This misalignment, which depends on temperature, conductivity and pressure, was partially corrected with the SBE Data Processing software *align* routine by advancing temperature +0.063 s relative to pressure. Then, a low-pass filter was applied to pressure, conductivity and temperature to smooth high frequency data. The main issue was the modeling of the thermal inertia effects within the conductivity cell (Lueck, 1990; Lueck and Picklo, 1990), which induces changes in the derived salinity values. These thermal effects are contemplated in the algorithmic *cell-thermal mass* of the SBE Data Processing software, through the coefficients α (initial magnitude of the fluid thermal anomaly) and β^{-1} (relaxation time of the fluid thermal anomaly). The salinity signal after applying both the standard SBE coefficients ($\alpha = 0.03$ and $\beta^{-1} = 7$) and those proposed by Lueck and Picklo (1990) ($\alpha = 0.028$ and $\beta^{-1} = 9$) was very similar. The highest difference between the salinity profiles before and after applying the *cell-thermal mass* algorithm (0.03 psu) was found at the depth of the pycnocline (z~ 38 m). Modeling the anomaly was particularly challenging for the sawtooth profiles considering the results from Lueck and Picklo (1990), who found that the anomaly persists 45 s after crossing the thermocline. Following the manufacturer suggestions, it was decided not to apply the *cell-thermal mass* algorithm to the conductivity signal at all. Finally, the derived variables were calculated. Remaining salinity spikes could be related to shed wakes from the CTD package that mix up the surrounding water. Different experiments with the *median filter* routine on derived variables data were performed to minimize spiking. A window size of $3 \cdot 16\mathrm{Hz} = 48$ scans was used and the filter was applied consecutively three times for conductivity, temperature, salinity and density data.

6 Underway data

A linear least squares fit was made for each variable between the CTD profiles data extracted at the 2 dbar level during down- and up-cast and the underway data to determinate an *offset* and a *slope* for the underway data corrections. This calibration was performed using only CTD and underway data collected simultaneously in time and space (35 data points in total). Figure 3 shows the pre- and post-calibrated differences between CTD and underway data for each variable.

Commonly, spurious data can be recorded by pump malfunction that alters the flow of water through the internal conduits or by chemical or biological depositions in the measurement cells or filters. An inspection of the data was held and questionable data were rejected. Finally, to smooth the noise in the underway calibrated data caused by flow rate disturbances, temperature and conductivity were filtered by applying the *median filter* routine from the SBE Data Processing software, using a window size of 256 scans. This filter was carried out four times consecutively before the *derive* routine was applied.

7 ADCP data

The hull-mounted ADCP data was collected with the TRDI VMDAS software version 1.3. At the beginning of the cruise the vessel position was provided by a GPS Furuno GP-31, but no heading signal input was set. The problem was discovered on Feb. 6 at 0 h UTC after the late spring survey across the STF. Therefore, only along-track velocities can be used from this data. The ancillary navigation input was then modified and GPS directional Applanix POS MV data was then set as input for the heading and attitude data.

The transducer depth and the blanking interval were 3.93 m and 4 m, respectively. The ADCP data were set to profile with a vertical bin size of 4 m (50 bins total) with single-ping bottom track enabled to a maximum depth of 500 m, and a ping interval of 2 s between ensembles. The data were then averaged to 3 min temporal resolution (approximately 0.6 km in average).

The ADCP data was processed using CODAS (Common Oceanographic Data Access System) software system v.3.1 developed at the University of Hawaii (Firing, 1995), https://currents.soest.hawaii.edu/docs/adcp_doc/codas_doc/.

8 Lessons learned

Prepare a detailed list including all measurements to be made, along with methodology, sampling and analytical instrumentation (Pollard et al., 2011). Collection of ocean data of the highest possible quality requires careful Quality Control and Quality Assurance procedures for the underwater unit and all sensor components (https://www.oceanbestpractices.net/handle/11329/336). These control tasks should be carried out and if possible formally reported before the cruise starts.

The overall quality of CTD data collection depends on a number of factors, such as: sensor calibration; equipment performance; software configuration and bugs during acquisition and processing; hardware problem; etc.

The selection of instruments and sensors used for data acquisition was carried out before the cruise in the Québec – Ocean Laboratory (UQAR/ISMER, Canada). They checked sensors calibration and equipment performance to acquire the best pos-

sible hydrographic data. However, some system presented problems during the cruise as were documented in this paper. The control tasks will be more carefully checked in the next cruises.

9 Data availability

The hydrographic data sets are reported in comma-separated values (csv) format. CTD vertical profile data are reported at 1 dbar pressure intervals while underway surface temperature, salinity and fluorescence data, Scanfish II CTD and FLNTU data and shipboard ADCP data are reported in the original sampling frequency recorded in physical units. One file for section and for sensor is provided for each survey across the STF (e.g., file named T1_lst correspond to CTD data for transect 1 in late spring tide and T1_FLNTU_lst correspond to FLNTU data for transect 1 in late spring tide). ADCP data files are named according to the CODAS output. The data are currently available at the US National Oceanographic Data Center, NOAA, under https://doi.org/10.7289/V5MP51J2.

Appendix A: Scanfish II data gridding

Since the data collected from the Scanfish have non-uniform spacing in both horizontal and vertical, the calibrated and post-processed data of each section was transformed into a rectangular grid with a resolution of $593 - 610$ m in the horizontal and 0.6 m in the vertical for a better post-analysis. After testing several geometries, the final grid geometry followed two steps. The vertical limits were set to the minimum and maximum depth reached by the Scanfish, corresponding to 0.063 m and 85.131 m, respectively. Then, as the length of each section was different, for each of them, the horizontal limits begins and ends where a 'V-shaped' profile begins or ends. A 'V-shaped' profile is the sum of a consecutive down and up-cast of the Scanfish. Kriging method type point was used to interpolate the node values, with horizontal and vertical radius of 1.8 km and 1.2 m, respectively. Figure A1 focuses on one of the sections (T1) for late spring tide to illustrate the main features of the water column structure near the southern mouth of SJG, representative of average summer conditions.

Competing interests. The authors declare that they have no conflict of interest.

Acknowledgements. This program was financed by the Institut des sciences de la mer de Rimouski/Université du Québec à Rimouski (ISMER/UQAR) from Canada, the Consejo Nacional de Investigaciones Científicas y Técnicas (CONICET) and the Ministerio de Ciencia y Tecnología (MINCyT) from Argentina. We thank the Instituto Nacional de Investigación y Desarrollo Pesquero (INIDEP, Argentina) that made available the Autosal salinometer and the Laboratorio de Oceanografía Química y Contaminación de Aguas (LOQyCA, Argentina) for allowing the use of the water samples measurements of nutrients, pH and DO. We also acknowledge Valérie Massé-Beaulne's detailed explanation of the measurement of Chl concentrations. We thank the crew and scientific staff of R/V *Coriolis II*. Finally, we wish to acknowledge D. Valla for his useful comments and language editing.

References

Acha, E. M., Mianzan, H. W., Guerrero, R. A., Favero, M., and Bava, J.: Marine fronts at the continental shelves of austral South America: Physical and ecological processes, Journal of Marine Systems, 44, 83 – 105, doi:https://doi.org/10.1016/j.jmarsys.2003.09.005, http://www.sciencedirect.com/science/article/pii/S0924796303001271, 2004.

Acha, E. M., Piola, A., Iribarne, O., and Mianzan, H.: Ecological processes at marine fronts: oases in the ocean, Springer, issn 2191-5555 (electronic) edn., 2015.

Alemany, D., Acha, E. M., and Iribarne, O.: The relationship between marine fronts and fish diversity in the Patagonian Shelf Large Marine Ecosystem, Journal of Biogeography, 36, 2111–2124, doi:10.1111/j.1365-2699.2009.02148.x, https://onlinelibrary.wiley.com/doi/abs/10.1111/j.1365-2699.2009.02148.x, 2009.

Alemany, D., Acha, E. M., and Iribarne, O. O.: Marine fronts are important fishing areas for demersal species at the Argentine Sea (Southwest Atlantic Ocean), Journal of Sea Research, 87, 56 – 67, doi:https://doi.org/10.1016/j.seares.2013.12.006, http://www.sciencedirect.com/science/article/pii/S1385110113002463, 2014.

Belkin, I., Cornillon, P., and Sherman, K.: Fronts in Large Marine Ecosystems, Progress in Oceanography - PROG OCEANOGR, 81, 223–236, doi:10.1016/j.pocean.2009.04.015, 2009.

Brown, J., Fernand, L., and Hill, A. E.: Scanfish: high performance towed undulator, Sea Technology, 37, 23–28, 1996.

Campagna, C., Sanderson, E. W., Coppolillo, P. B., Falabella, V., Piola, A. R., Strindberg, S., and Croxall, J. P.: A species approach to marine ecosystem conservation, Aquatic Conservation: Marine and Freshwater Ecosystems, 17, S122–S147, doi:10.1002/aqc.918, https://onlinelibrary.wiley.com/doi/abs/10.1002/aqc.918, 2007.

Carbajal, J. C., Rivas, A. L., and Chavanne, C.: High-Frequency Frontal Displacements South of San Jorge Gulf During a Tidal Cycle Near Spring and Neap Phases: Biological Implications Between Tidal States, Oceanography, 31, https://doi.org/10.5670/oceanog.2018.411, 2018.

Carpenter, J. H.: The Accuracy of the Winkler Method for dissolved Oxygen analysis, Limnology and Oceanography, 10, 135–140, doi:10.4319/lo.1965.10.1.0135, http://dx.doi.org/10.4319/lo.1965.10.1.0135, 1965.

Cartwright, D. E. and Ray, R. D.: Energetics of global ocean tides from Geosat altimetry, Journal of Geophysical Research: Oceans, 96, 16 897–16 912, doi:10.1029/91JC01059, https://agupubs.onlinelibrary.wiley.com/doi/abs/10.1029/91JC01059, 1991.

Egbert, G. D. and Ray, R. D.: Estimates of M2 tidal energy dissipation from TOPEX/Poseidon altimeter data, Journal of Geophysical Research: Oceans, 106, 22 475–22 502, doi:10.1029/2000JC000699, https://agupubs.onlinelibrary.wiley.com/doi/abs/10.1029/2000JC000699, 2001.

Firing, E.: Processing ADCP data with the CODAS software system version 3.1, Joint Institute for Marine and Atmospheric Research, University of Hawaii & National Oceanographic Data Center., 1995.

Forbes, M. C. and Garraffo, Z. D.: A note on the mean seasonal transport on the Argentinian shelf, Journal of Geophysical Research: Oceans, 93, 2311–2319, doi:10.1029/JC093iC03p02311, https://agupubs.onlinelibrary.wiley.com/doi/abs/10.1029/JC093iC03p02311, 1988.

Glembocki, N. G., Williams, G. N., Góngora, M. E., Gagliardini, D. A., and Orensanz, J. M. L.: Synoptic oceanography of San Jorge Gulf (Argentina): A template for Patagonian red shrimp (Pleoticus muelleri) spatial dynamics, Journal of Sea Research, 95, 22 – 35, doi:https://doi.org/10.1016/j.seares.2014.10.011, http://www.sciencedirect.com/science/article/pii/S1385110114001841, 2015.

Glorioso, P. D. and Flather, R. A.: A barotropic model of the currents off SE South America, Journal of Geophysical Research: Oceans, 100, 13 427–13 440, doi:10.1029/95JC00942, http://dx.doi.org/10.1029/95JC00942, 1995.

Glorioso, P. D. and Flather, R. A.: The Patagonian Shelf tides, Progress in Oceanography, 40, 263 – 283, doi:http://dx.doi.org/10.1016/S0079-6611(98)00004-4, http://www.sciencedirect.com/science/article/pii/S0079661198000044, tidal Science In Honour of David E. Cartwright, 1997.

Guildline Instruments: Technical manual for Model 9400B "Autosal", Tech. rep., TM8400B-L-00, revised November 2006, Guildline Instruments, Smith Falls, Ontario, Canada, 71 pp, 2004.

Landeira, J. M., Ferron, B., Lunven, M., Morin, P., Marié, L., and Sourisseau, M.: Biophysical Interactions Control the Size and Abundance of Large Phytoplankton Chains at the Ushant Tidal Front, PLOS ONE, 9, 1–14, doi:10.1371/journal.pone.0090507, https://doi.org/10.1371/journal.pone.0090507, 2014.

Lueck, R. G.: Thermal Inertia of Conductivity Cells: Theory, Journal of Atmospheric and Oceanic Technology, 7, 741–755, doi:10.1175/1520-0426(1990)007<0741:TIOCCT>2.0.CO;2, 1990.

Lueck, R. G. and Picklo, J. J.: Thermal Inertia of Conductivity Cells: Observations with a Sea-Bird Cell, Journal of Atmospheric and Oceanic Technology, 7, 756–768, doi:10.1175/1520-0426(1990)007<0756:TIOCCO>2.0.CO;2, 1990.

Miller, G. R.: The flux of tidal energy out of the deep oceans, Journal of Geophysical Research, 71, 2485–2489, doi:10.1029/JZ071i010p02485, https://agupubs.onlinelibrary.wiley.com/doi/abs/10.1029/JZ071i010p02485, 1966.

Miloslavich, P., Klein, E., Díaz, J. M., Hernández, C. E., Bigatti, G., Campos, L., Artigas, F., Castillo, J., Penchaszadeh, P. E., Neill, P. E., Carranza, A., Retana, M. V., Díaz de Astarloa, J. M., Lewis, M., Yorio, P., Piriz, M. L., Rodríguez, D., Yoneshigue-Valentin, Y., Gamboa, L., and Martín, A.: Marine Biodiversity in the Atlantic and Pacific Coasts of South America: Knowledge and Gaps, PLOS ONE, 6, 1–43, doi:10.1371/journal.pone.0014631, https://doi.org/10.1371/journal.pone.0014631, 2011.

Moreira, D., Simionato, C., and Dragani, W.: Modeling ocean tides and their energetics in the North Patagonia Gulfs of Argentina, Journal of Coastal Research, 27, 87–102, 2011.

Palma, E. D., Matano, R. P., and Piola, A. R.: A numerical study of the Southwestern Atlantic Shelf circulation: Barotropic response to tidal and wind forcing, Journal of Geophysical Research: Oceans, 109, n/a–n/a, doi:10.1029/2004JC002315, http://dx.doi.org/10.1029/2004JC002315, c08014, 2004.

Parsons, T., Maita, Y., and Lalli, C.: Manual of chemical and biological methods for seawater analysis, in: Manual of chemical and biological methods for seawater analysis, Pergamon, 1984.

Pollard, R. T., Moncoiffé, G., and O'Brien, T. D.: The IMBER Data Management Cookbook - A Project Guide to good Data practices, IMBER Report No. 3, IPO Secretariat, Plouzané, France, 16pp, 2011.

Rivas, A. L.: Spatial variation of the annual cycle of temperature in the Patagonian shelf between 40 and 50° of south latitude, Continental Shelf Research, 14, 1539 – 1554, doi:https://doi.org/10.1016/0278-4343(94)90089-2, http://www.sciencedirect.com/science/article/pii/0278434394900892, 1994.

Romero, S. I., Piola, A. R., Charo, M., and Garcia, C. A. E.: Chlorophyll-a variability off Patagonia based on SeaWiFS data, Journal of Geophysical Research: Oceans, 111, doi:10.1029/2005JC003244, https://agupubs.onlinelibrary.wiley.com/doi/abs/10.1029/2005JC003244, 2006.

Satlantic LP: Operation Manual for MBARI-ISUS V3, Satlantic, Richmond Terminal, Pier 9, 3481 North Marginal Road, Halifax, Nova Scotia, Canada, revision a.8 edn., 2012.

Sea-Bird Electronics Inc: Application note NO.31.Computing Temperature and Conductivity Slope and Offset Correction. Coefficients from Laboratory Calibrations and Salinity Bottle Samples, 13431 NE 20th Street Bellevue, WA 98005, USA, 2010.

Sea-Bird Electronics Inc: Application note NO.64-2. SBE 43 Dissolved Oxygen Sensor Calibration and Data Corrections, 13431 NE 20th Street Bellevue, WA 98005, USA, 2012.

Simpson, J. and Bowers, D.: Models of stratification and frontal movement in shelf seas, Deep Sea Research Part A. Oceanographic Research Papers, 28, 727 – 738, doi:https://doi.org/10.1016/0198-0149(81)90132-1, http://www.sciencedirect.com/science/article/pii/0198014981901321, 1981.

Skalar Analytical® V.B: Skalar Methods - Analysis: Nitrate + Nitrite - Catnr. 461-031 + DIAMOND Issue 081505/MH/99235956. Breda (The Netherlands), 2005a.

Skalar Analytical® V.B: Skalar Methods - Analysis: Phosphate - Catnr. 503-010w/r + DIAMOND Issue 081505/MH/99235956. Breda (The Netherlands), 2005b.

Skalar Analytical® V.B: Skalar Methods - Analysis: Silicate -Catnr. 563-051 + DIAMOND Issue 081505/MH/99235956. Breda (The Netherlands), 2005c.

Strickland, J. D. and Parsons, T. R.: A practical handbook of seawater analysis, Fisheries Research Board of Canada, 116 Lisgar Street, Ottawa, Canada, second edition (bulletin 167) edn., 1972.

Sylwan, C. A.: Geology of the Golfo San Jorge Basin, Argentina. Geología de la Cuenca del Golfo San Jorge, Argentina., Journal of Iberian Geology, 27, http://revistas.ucm.es/index.php/JIGE/article/view/JIGE0101110123A, 2001.

Tonini, M., Palma, E., and Rivas, A.: Modelo de alta resolución de los Golfos Patagónicos, Mecánica Computacional, 25, 1441–1460, 2006.

Twardowski, M., Lewis, M., Barnard, A., and Zaneveld, J.: Remote Sensing of Coastal Aquatic Waters, pp. 69–100, 2005.

UNESCO IWG: The practical salinity scale1978 and the international equation of state of seawater 1980, Tenth Report of the Joint Panel on Oceanographic Tables and Standards (JPOTS), p. 25, 1981.

Webb, D.: On the age of the semi-diurnal tide, Deep Sea Research and Oceanographic Abstracts, 20, 847 – 852, doi:https://doi.org/10.1016/0011-7471(73)90006-5, http://www.sciencedirect.com/science/article/pii/0011747173900065, 1973.

Table 1. Summary of the sensors used on board R/V *Coriolis II* in MARES leg 2 (Feb. 4-10 2014).

Instrument	Sensor	Model	Serial #	Calibration date
SBE911*plus*	Temperature	SBE3*plus*	5769	Oct.22 2013
(CTD profile)	Pressure	Digiquartz with TC	1168	Nov.19 2013
	Conductivity	SBE4	4244	Nov.06 2013
	Oxygen	SBE43	2766	Nov.15 2013
	pH	SBE18	1078	Nov.20 2013
	Fluorescence	ECO FL WetLabs	FLRT-3363	Nov.11 2013
	Nutrients	Satlantic MBARI-ISUS	0184	May.25 2013
	PAR	Biospherical/Licor	70455	Nov.04 2013
	Beam transmission	WetLabs C-Star	CST-1628PR	Jun.11 2013
	Altimeter	PSA-916	61114	-
SBE49FastCAT	Temperature		0226	Jan.17 2011
(Scanfish II)	Pressure	Strain gauge	0226	Jan.14 2011
	Conductivity		0226	Jan.17 2011
	Fluorescence/Turbidity	ECO FLNTU WetLabs	FLNTURT-2037	Oct.07 2010
SBE19*plus*	Temperature		4975	Mar.07 2013
(Underway)	Pressure	Strain gauge	4975	Feb.28 2013
	Conductivity		4975	Mar.01 2013
	Fluorescence	Seapoint Chlorophyll Fluorometer	2803	Apr.28 2006

Table 2. Field measurements across the STF using the towed undulating vehicle Scanfish II. Arrows indicate the cruise path parallel to each transect ($\Rightarrow$: offshore the Gulf, $\Leftarrow$: into the Gulf). Δx represents the transect length.

	Transect	Path	Begin		End		Depth range (m)	Δx (km)	# Scans
			Date (hh:mm)	lat./lon. (°)	Date (hh:mm)	lat./lon. (°)			
late spring tide	T1	$\Rightarrow$	Feb.5 (07:38)	-46.512,-65.970	(10:01)	-46.614,-65.709	0.83-79.87	24.0	114505
	T2	$\Leftarrow$	(10:13)	-46.592,-65.697	(12:10)	-46.462,-66.015	2.40-81.36	28.8	111801
	T3	$\Rightarrow$	(12:21)	-46.441,-65.996	(13:55)	-46.538,-65.742	2.73-79.95	22.4	90001
	T4	$\Leftarrow$	(14:08)	-46.512,-65.734	(15:48)	-46.418,-65.961	6.11-79.96	21.2	96002
	T5	$\Rightarrow$	(15:59)	-46.401,-65.936	(17:43)	-46.513,-65.653	6.81-80.24	25.4	99601
	T6	$\Leftarrow$	(17:59)	-46.488,-65.636	(19:23)	-46.398,-65.862	4.17-79.74	20.4	81201
intermediate tide	T1-1	$\Rightarrow$	Feb.8 (23:58)	-46.502,-65.997	Feb.9 (01:32)	-46.598,-65.755	0.50-82.97	21.8	90003
	T1-2	$\Leftarrow$	(01:46)	-46.596,-65.759	(02:55)	-46.518,-65.953	1.54-84.37	17.4	66001
	T1-3	$\Rightarrow$	(03:05)	-46.518,-65.967	(04:37)	-46.612,-65.720	1.30-82.71	22.1	88001
	T1-4	$\Leftarrow$	(04:45)	-46.614,-65.710	(06:46)	-46.496,-66.012	2.66-80.68	27.3	116001
	T1-5	$\Rightarrow$	(07:07)	-46.499,-66.004	(08:45)	-46.612,-65.718	2.74-80.44	25.5	94002
	T1-6	$\Leftarrow$	(09:00)	-46.615,-65.700	(11:19)	-46.485,-66.036	2.04-85.13	30.4	134002
early neap tide	T1	$\Rightarrow$	(11:34)	-46.484,-66.036	(13:48)	-46.615,-65.709	4.36-80.24	29.7	128801
	T2	$\Leftarrow$	(14:02)	-46.589,-65.696	(16:00)	-46.462,-66.013	2.37-80.38	28.6	114001
	T3	$\Rightarrow$	(16:13)	-46.440,-65.997	(18:06)	-46.563,-65.681	2.65-80.34	28.3	108801
	T4	$\Leftarrow$	(18:20)	-46.542,-65.659	(21:02)	-46.394,-66.028	2.49-81.49	34.0	156001
	T5	$\Rightarrow$	(21:17)	-46.373,-66.009	(23:26)	-46.513,-65.652	0.06-80.27	32.0	124002
	T6	$\Leftarrow$	(23:40)	-46.492,-65.633	Feb.10 (04:13)	-46.225,-66.334	1.71-83.93	63.1	262406

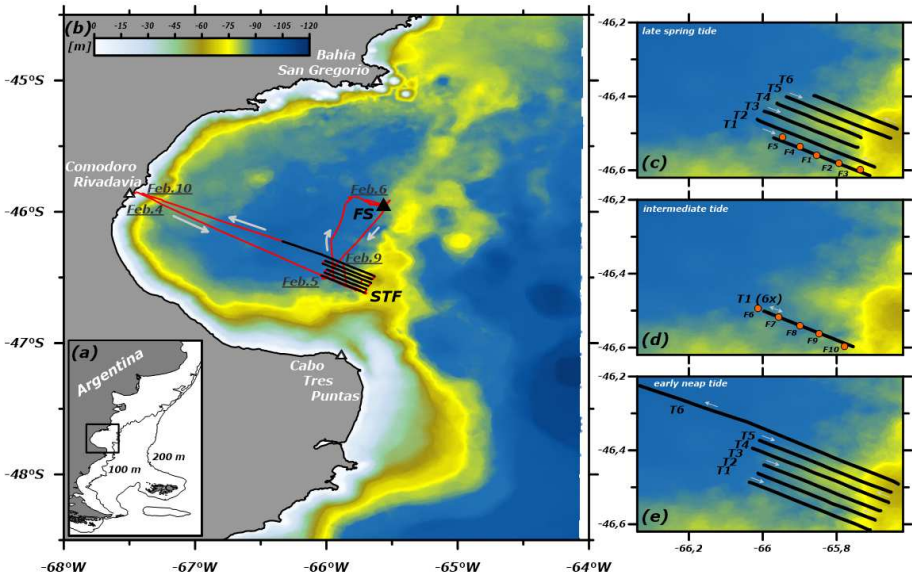

Figure 1. Study area (a) Patagonia shelf; (b) San Jorge Gulf, the underway track for MARES leg 2 (red line), the Scanfish transects across the STF (black lines) and the FS (black triangle). A zoom of the survey across the STF for (c) late spring tide, (d) intermediate tide, showing the CTD vertical profiles (orange circles); and (e) for early neap tide. Bathymetry is shown as shaded colors, highlighting the bank south of the Gulf, where depths range from 45 to 75 m. Arrows in light gray indicate the cruise path, particularly in d) the double arrow references the survey back and forth over T1. STF: Southern Tidal Front. FS: Fixed Station.

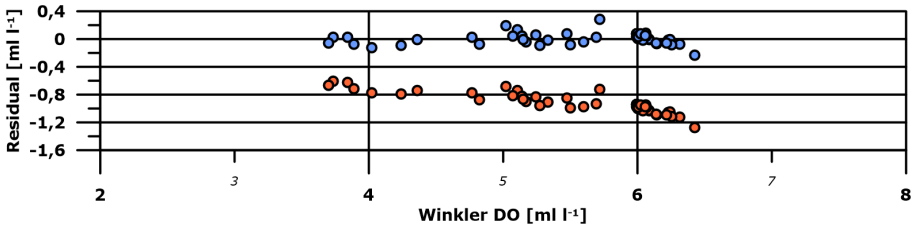

Figure 2. Distribution of dissolved oxygen residuals versus dissolved oxygen concentration (both in $\mathrm{ml\,l^{-1}}$), before (orange dots) and after (blue dots) the SBE43 sensor calibration.

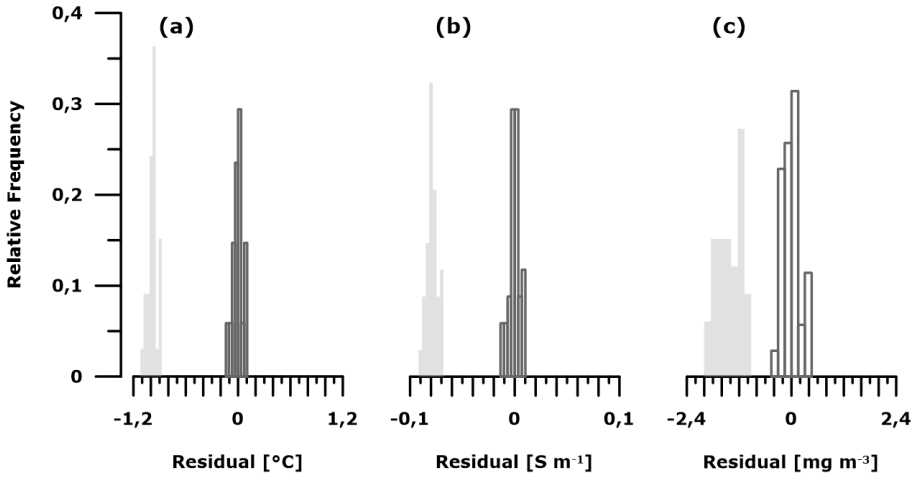

Figure 3. Relative frequency of (a) temperature, (b) conductivity and (c) fluorescence residuals before (gray shaded bars) and after (black solid bars) the underway calibrations.

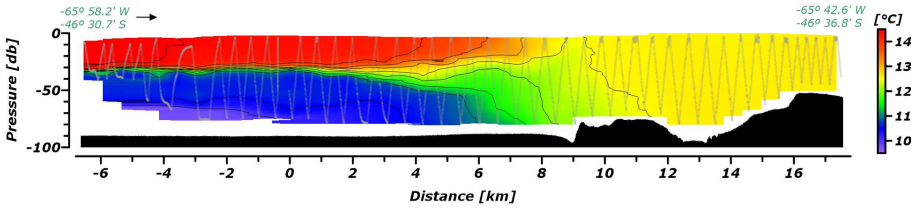

Figure A1. Vertical section of temperature in late spring tide for transect 1. The horizontal scale represents distance in km from an arbitrary zero position, whereas the profile of the seabed is derived from the ship echo-sounder EK60. The consecutive 'V-shaped' profiles of the Scansifh II are marked in gray, with a dot every 10 data points, and the cruise path with a black arrow.